Chemical Science

ROYAL SOCIETY OF CHEMISTRY

EDGE ARTICLE

View Article Online
View Journal | View Issue

Cite this: *Chem. Sci.*, 2024, **15**, 16069

All publication charges for this article have been paid for by the Royal Society of Chemistry

Dinitrogen reduction chemistry with scandium provides a complex with two side-on $(N{=}N)^{2-}$ ligands bound to one metal: $(C_5Me_5)Sc[(\mu\text{-}\eta^2{:}\eta^2\text{-}N_2)Sc(C_5Me_5)_2]_2$†

Joshua D. Queen, [a] Ahmadreza Rajabi, [a] Quinn E. Goudzwaard, [a] Qiong Yuan, [b] Dang Khoa Nguyen, [a] Joseph W. Ziller, [a] Filipp Furche, *[a] Zhenfeng Xi *[b] and William J. Evans *[a]

Although there are few reduced dinitrogen complexes of scandium, this metal has revealed a new structural type in reductive dinitrogen chemistry by reduction of bis(pentamethylcyclopentadienyl) scandium halides under N_2. Reduction of Cp^*_2ScI ($Cp^* = C_5Me_5$) with potassium graphite (KC_8) under dinitrogen generates the dark blue paramagnetic complex $(Cp^*_2Sc)_2(\mu\text{-}\eta^1{:}\eta^1\text{-}N_2)$, **1**. This end-on bridging $(N{=}N)^{2-}$ complex is a diradical with a magnetic moment of 2.8μ_B. Upon further reduction of **1** with KC_8, the orange diamagnetic trimetallic complex $Cp^*Sc[(\mu\text{-}\eta^2{:}\eta^2\text{-}N_2)ScCp^*_2]_2$, **2**, is obtained. This complex has an unprecedented structure in which two side-on bridging $(N{=}N)^{2-}$ ligands are bound to the central $(Cp^*Sc)^{2+}$ moiety. Complex **2** can also be obtained directly from reduction of Cp^*_2ScI or a mixture of Cp^*_2ScCl and $Cp^*_2ScCl(THF)$ with KC_8. The reaction of Cp^*_2ScI with KC_8 in the presence of 18-crown-6 or 2.2.2-cryptand affords **2** along with small amounts of $Cp^*_2Sc(\mu\text{-}\eta^2{:}\eta^2\text{-}N_2)ScCp^*I(THF)$, **3**, which is green at room temperature and purple at low temperature and displays a mixture of side-on and end-on bridging isomers in the crystal structure collected at −180 °C. Density functional theory (DFT) calculations are consistent with a triplet ground state for the end-on complex **1** and singlet ground states for the side-on complexes **2** and **3**.

Received 17th June 2024
Accepted 29th August 2024

DOI: 10.1039/d4sc03977g

rsc.li/chemical-science

Introduction

Metal dinitrogen complexes are an important class of compounds that are of interest for chemical processes that require reduction of the inert N_2 molecule.[1–5] The first reported N_2 complex, the monometallic $[Ru(NH_3)_5(N_2)]^{2+}$, was found to have a terminal end-on bound dinitrogen ligand.[6] Subsequently, bimetallic complexes with bridging dinitrogen ligands were discovered which had both end-on and side-on coordination of the N_2 unit.[7–10] There are now hundreds of examples of crystallographically characterized metal dinitrogen compounds[9] with approximately 600 terminal compounds, 500 bridging end-on examples, and almost 100 side-on complexes reported in the Cambridge Structural Database.[11] With such an extensive effort on this topic, it is unusual to find new structural types of reduced dinitrogen complexes.

Although metal dinitrogen chemistry has been heavily studied, for the first member of the transition metal series, scandium, only three structurally characterized examples of dinitrogen complexes have been reported to date, Fig. 1.[12–14] The first of these, $[(C_5Me_4H)_2Sc]_2(\mu\text{-}\eta^2{:}\eta^2\text{-}N_2)$,[12] had a side-on bridging $(N{=}N)^{2-}$ ligand with a planar Sc_2N_2 core that was the hallmark of rare-earth element (Sc, Y, and the lanthanides) dinitrogen complexes from 1988 until 2017.[15–26]

However, the second example, $[K(crypt)]_2\{[(R_2N)_3Sc]_2(\mu\text{-}\eta^1{:}\eta^1\text{-}N_2)\}$ (crypt = 2.2.2-cryptand, R = $SiMe_3$), was ground-breaking in that it revealed the first end-on bridging coordination mode for a rare-earth $(N{=}N)^{2-}$ complex[13] and was found to readily revert to its Sc(II) amide precursor, $[K(crypt)][Sc(NR_2)_3]$ with exposure to light. Subsequently, it was found with the larger rare-earth metal analogs of this amide-ligated compound that the dianonic $\{[(R_2N)_3Ln]_2(\mu\text{-}\eta^x{:}\eta^x\text{-}N_2)\}^{2-}$ complexes could contain mixtures of end-on and side-on isomers in the solid state, *i.e.* $x = 1,2$ for Ln = Nd, Gd.[27,28] It is relevant to results reported here that single crystals of the Nd compound were found to isomerize on the diffractometer at around −90 °C.

[a]*Department of Chemistry, University of California, Irvine, 92697, California, USA. E-mail: jqueen@uci.edu; arajabis@uci.edu; qgoudzwa@uci.edu; khoan16@uci.edu; wevans@uci.edu; filipp.furche@uci.edu; jziller@uci.edu*

[b]*Beijing National Laboratory for Molecular Sciences (BNLMS), Key Laboratory of Bioorganic Chemistry and Molecular Engineering of Ministry of Education, College of Chemistry, Peking University, Beijing 100871, China. E-mail: yuanqiongyin@pku.edu.cn; zfxi@pku.edu.cn*

† Electronic supplementary information (ESI) available. CCDC 2324189, 2344840, 2344841 and 2348488–2348490. For ESI and crystallographic data in CIF or other electronic format see DOI: https://doi.org/10.1039/d4sc03977g

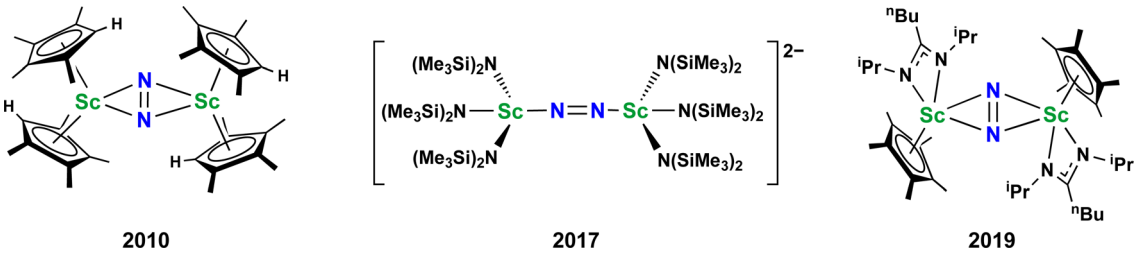

Fig. 1 Previously reported dinitrogen compounds of scandium. In all cases the N_2 is reduced to an $(N{=}N)^{2-}$ ligand.

The third example of a reduced dinitrogen complex of scandium, a side-on complex with a mixed ligand cyclopentadienyl amidinate coordination environment, $\{[^{n}BuC(N^{i}Pr)_2]Cp^*Sc\}_2(\mu\text{-}\eta^2{:}\eta^2\text{-}N_2)$ ($Cp^* = C_5Me_5$),[14] was also special. This complex could be reduced further to the $(N_2)^{3-}$ species, $[\{[^{n}BuC(N^{i}Pr)_2]Cp^*Sc\}_2(\mu\text{-}\eta^2{:}\eta^2\text{-}N_2)]^{1-}$,[14] chemistry that had to that point only been observed for the bis(silyl)amido compounds $\{[(R_2N)_2(THF)Ln]_2(\mu\text{-}\eta^2{:}\eta^2\text{-}N_2)\}^{1-}$.[29,30] Furthermore, the $[\{[^{n}BuC(N^{i}Pr)_2]Cp^*Sc\}_2(\mu\text{-}\eta^2{:}\eta^2\text{-}N_2)]^{1-}$ complex could be stepwise functionalized at the bridging nitrogen to release hydrazine derivatives.[14]

We now report a new structural type of reduced dinitrogen complex previously unobserved with any metal by studying the reduction of bis(pentamethylcyclopentadienyl) scandium halides. Recently we reported that treating Cp^*_2ScI with KC_8 generates a Sc(II) compound with spectroscopic features similar to those of the first stable scandium metallocene, Cp^{ttt}_2Sc ($Cp^{ttt} = C_5H_2{}^{t}Bu_3$).[31] However, the product of the Cp^*_2ScI/KC_8 reaction, which forms red solutions at −78 °C under argon and is possibly the scandocene Cp^*_2Sc, is highly reactive with arene and ether solvents through C–H or C–O bond activation. To further understand the nature of the Cp^*_2ScI/KC_8 reduction product, we investigated its reactivity with N_2. This has resulted in the isolation of the first neutral end-on bridging dinitrogen complex of scandium, $(Cp^*_2Sc)_2(\mu\text{-}\eta^1{:}\eta^1\text{-}N_2)$, **1**.

The subsequent treatment of **1** with KC_8, rather than forming a stable compound containing an $(N_2)^{3-}$ anion, gave the trimetallic complex $Cp^*Sc[(\mu\text{-}\eta^2{:}\eta^2\text{-}N_2)ScCp^*_2]_2$, **2**. To our knowledge, this is the first example of a complex containing two side-on dinitrogen ligands attached to a single metal. Previously, a bimetallic mixed-valent titanium complex with two bridging $(N{=}N)^{2-}$ ligands connecting the metals, $\{[(R_2N)_2Ti]_2(\mu\text{-}\eta^2{:}\eta^2\text{-}N_2)_2\}^{1-}$ (R = $SiMe_3$) was reported,[32] but reanalysis of this product revealed it to be the toluene inverse sandwich complex $\{[(R_2N)_2Ti]_2(\mu\text{-}C_6H_5Me)\}^{1-}$.[33] Complexes with two end-on dinitrogen ligands per metal are known [9] such as $[Cp^*_2(\eta^1\text{-}N_2)Zr]_2(\mu\text{-}\eta^1{:}\eta^1\text{-}N_2)$[34] and $[(Nacnac)Cr(\mu\text{-}\eta^1{:}\eta^1\text{-}N_2)]_x$ (x = 3, 4; Nacnac = $HC\{MeCN(2,6\text{-}Me_2C_6H_3)\}_2$).[35] However, multiple side-on coordination to a single metal center has so-far been elusive. In the course of these experiments we also identified the mixed ligand cyclopentadienyl halide complex, $Cp^*_2Sc(\mu\text{-}\eta^x{:}\eta^x\text{-}N_2)ScCp^*I(THF)$, **3** ($x$ = 1, 2), which displays temperature dependent side-on/end-on isomerization and has primarily a side-on structure with some end-on disorder in the solid state.

Results

$(Cp^*_2Sc)_2(\mu\text{-}\eta^1{:}\eta^1\text{-}N_2)$, 1

The end-on bridging dinitrogen complex, $(Cp^*_2Sc)_2(\mu\text{-}\eta^1{:}\eta^1\text{-}N_2)$, **1**, was prepared by reduction of Cp^*_2ScI with potassium graphite (KC_8) under a N_2 atmosphere according to eqn (1). Upon addition of KC_8 to a stirred yellow solution of Cp^*_2ScI in Et_2O, a dark blue solution immediately forms. Repeated extractions of the resulting mixture with Et_2O followed by removal of the solvent under reduced pressure gives **1** as a dark blue powder in *ca.* 80% yield. Storage of a saturated Et_2O solution of **1** at −35 °C afforded dark blue-purple crystals that were suitable for X-ray diffraction.

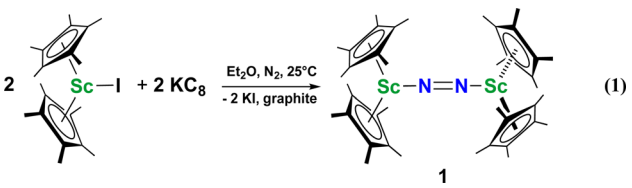

The structure of **1**, Fig. 2, shows that the overall molecular structure has a tetrahedral arrangement of the four Cp* ligand ring centroids which are all equivalent through crystallographic symmetry. A small positional disorder of the Sc atom site in the structure of **1** suggests the presence of a co-crystallized *ca.* 5% impurity of $(Cp^*_2Sc)_2(\mu\text{-}O)$, which is discussed in a later section. Co-crystallization of $(O)^{2-}$ oxide side products with rare-earth element $(N{=}N)^{2-}$ complexes has previously been observed[28] and attempts to independently prepare this oxide are discussed later.

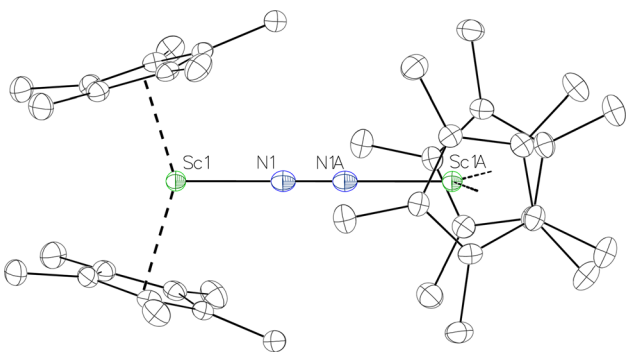

Fig. 2 Thermal ellipsoid plot (30%) of $(Cp^*_2Sc)_2(\mu\text{-}\eta^1{:}\eta^1\text{-}N_2)$, **1**, with hydrogen atoms and disordered Sc atoms not shown for clarity.

Table 1 Summary of the N–N bond lengths and N–N vibrational frequencies in end-on bridging rare-earth element compounds

Compound	N–N bond length (Å)	Raman shift (cm^{-1})	Ref.
$(Cp^*_2Sc)_2(\mu\text{-}\eta^1\text{:}\eta^1\text{-}N_2)$, **1**	1.174(5)	1595	This work
$[K(crypt)]_2\{[(R_2N)_3Sc]_2(\mu\text{-}\eta^1\text{:}\eta^1\text{-}N_2)\}^a$	1.221(3)	1644	13
$[K(crypt)]_2\{[(R_2N)_3Y]_2(\mu\text{-}\eta^1\text{:}\eta^1\text{-}N_2)\}^a$	1.216(7), 1.229(7)	1635	27
$[K(crypt)]_2\{[(R_2N)_3Tb]_2(\mu\text{-}\eta^1\text{:}\eta^1\text{-}N_2)\}^a$	1.217(3)	1623	28
$(Cp^{ttt}_2Gd)_2(\mu\text{-}\eta^1\text{:}\eta^1\text{-}N_2)$	1.130(8)	1623	36
$(Cp^{ttt}_2Tb)_2(\mu\text{-}\eta^1\text{:}\eta^1\text{-}N_2)$	1.175(8)	1621	36
$(Cp^{ttt}_2Dy)_2(\mu\text{-}\eta^1\text{:}\eta^1\text{-}N_2)$	1.215(13)	1618	36

[a] $R = SiMe_3$.

The Sc–Cent (Cent = Cp* ring centroid) distance in **1** is 2.17 Å with a Cent–Sc–Cent angle of 146.7°. The analogous metrical parameters in the side-on complex, $[(C_5Me_4H)_2Sc]_2(\mu\text{-}\eta^2\text{:}\eta^2\text{-}N_2)$,[12] are 2.20 Å and 131.0°. The Sc–N–N–Sc core in **1** is strictly linear, enforced by crystallographic symmetry, and has a 2.049(3) Å Sc–N distance. The 1.174(5) Å N–N distance is on the shorter end of the range of N–N distances reported for end-on bridging rare-earth element $(N_2)^{2-}$ compounds (Table 1). In comparison, the end-on $(N{=}N)^{2-}$ complex $[K(crypt)]_2\{[(R_2N)_3Sc]_2(\mu\text{-}\eta^1\text{:}\eta^1\text{-}N_2)\}$ has Sc–N distances of 2.032(2) and 2.030(2) Å, an N–N bond length of 1.221(3) Å, and Sc–N–N angles of 178.2(2) and 179.7(2)°.

We note that the crystallographically determined N–N bond lengths in rare-earth metal dinitrogen compounds can be variable between crystals of the same compound, whereas the N–N stretching frequency is consistent between samples.[37] The Raman spectrum of **1** shows the N–N stretching vibration at 1595 cm^{-1} which is less than that of $\{[(R_2N)_3Sc]_2(\mu\text{-}\eta^1\text{:}\eta^1\text{-}N_2)\}^{2-}$ at 1644 cm^{-1} and closer to the *ca.* 1620 cm^{-1} stretch for the neutral end-on bridging complexes $(Cp^{ttt}_2Ln)_2(\mu\text{-}\eta^1\text{:}\eta^1\text{-}N_2)$ (Ln = Gd, Tb, Dy),[36] Table 1.

Compound **1** is a diradical and has a broad ^1H NMR signal at 29 ppm in C_6D_6. The magnetic moment was determined by Evans' method NMR measurement[38–40] to be $2.8\mu_B$, consistent with the $2.83\mu_B$ spin-only magnetic moment expected for two unpaired electrons. Density functional theory calculations are in agreement with a predicted triplet ground state and are described further in the Computational Details section.

Compound **1** is soluble in hexane, benzene, toluene, and Et_2O, but upon dissolving in THF the dark blue color immediately fades to pale yellow. The thermal stability of **1** in solution was investigated by heating a C_6D_6 solution of **1** inside a J-Young NMR tube sealed under N_2. The filled portion of the NMR tube was immersed in a 100 °C oil bath and over 6 hours the intense blue solution faded to pale yellow. The ^1H NMR spectrum of this solution revealed the presence of a new Cp* methyl resonance at 1.73 ppm consistent with the formation of $Cp^*_2Sc(C_6D_5)$.[41] Signals corresponding to $Cp^*_2Sc(OEt)$[31] were also seen, which could result from reactions with trace amounts of Et_2O present in the sample. We previously found that these phenyl and ethoxide products formed from C–H and C–O bond activation of benzene or Et_2O by the Cp^*_2ScI/KC_8 reduction system in these solvents.[31] The other expected products from these reactions, Cp^*_2ScD and Cp^*_2ScEt, were not observed as they are expected to react further with the C_6D_6 solvent.[41] In the solid state, **1** was found to melt over the range of 183–187 °C during which the color changed to red. Gas evolution was observed and the red melt quickly decomposed to a white solid. These results are consistent with the liberation of dinitrogen upon thermolysis of **1** and concomitant formation of Cp^*_2Sc although this highly reactive species has not yet been isolated.

The stability of **1** towards photolysis was also examined, as $[K(crypt)]_2\{[(R_2N)_3Sc]_2(\mu\text{-}\eta^1\text{:}\eta^1\text{-}N_2)\}$ was found to eliminate N_2 under ambient light.[13] Solutions of **1** in C_6D_6 sealed under N_2 showed no decomposition products when the samples were left on the benchtop for a week. One of these samples in a quartz tube was irradiated with a mercury arc lamp with a 200–400 nm emission range for 4 hours and no formation of Cp^*_2ScPh or other products were observed in the ^1H NMR spectrum.

$Cp^*Sc[(\mu\text{-}\eta^2\text{:}\eta^2\text{-}N_2)ScCp^*_2]_2$, 2

The reduction of complex **1** was attempted with the aim of forming a $[(Cp^*_2Sc)_2(\mu\text{-}N_2)]^{1-}$ product containing an $(N_2)^{3-}$ moiety.[14,29,30] Treating an Et_2O solution of **1** and 18-crown-6 with 1 equiv. of KC_8 under a dinitrogen atmosphere resulted in a gradual color change to dark orange. Evaporation of the supernatant solution gave orange-brown crystals which were identified by X-ray diffraction as the trimetallic complex $Cp^*Sc[(\mu\text{-}\eta^2\text{:}\eta^2\text{-}N_2)ScCp^*_2]_2$, **2**, Fig. 3. To our knowledge, complexes with two side-on dinitrogen ligands bound to a single metal have not been previously reported. The deliberate synthesis of **2** from **1** was found to proceed in high yield according to the stoichiometry in Scheme 1. Although the intermediates are not yet understood, this reaction can be balanced by the reduction of an additional equivalent of N_2 to $(N{=}N)^{2-}$ and elimination of KCp*.

Alternatively, **2** could be prepared in a "one-pot" fashion from halide precursors, Scheme 1. The reaction of 3 equiv. Cp^*_2ScI with 4 equiv. of KC_8 in Et_2O initially formed of a dark blue solution of **1** followed by a gradual change to orange. Complex **2** was also prepared independently by reduction of a mixture of the chloride precursors Cp^*_2ScCl and $Cp^*_2ScCl(THF)$ in toluene. Initially, $ScCl_3$ was combined with 2 equiv. of KCp* in THF. Exchange of the reaction solvent to toluene and treatment of the resulting mixture with KC_8 under dinitrogen at room temperature led to the isolation of complex **2**. The

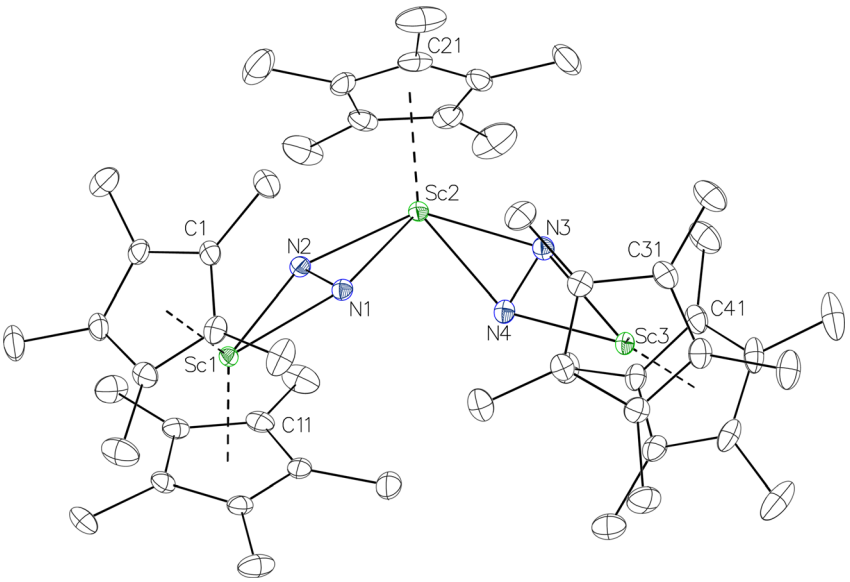

Fig. 3 Molecular structure of Cp*Sc[(μ-η²:η²-N_2)ScCp*$_2$]$_2$, **2** with thermal ellipsoids shown at 30% and hydrogen atoms omitted for clarity.

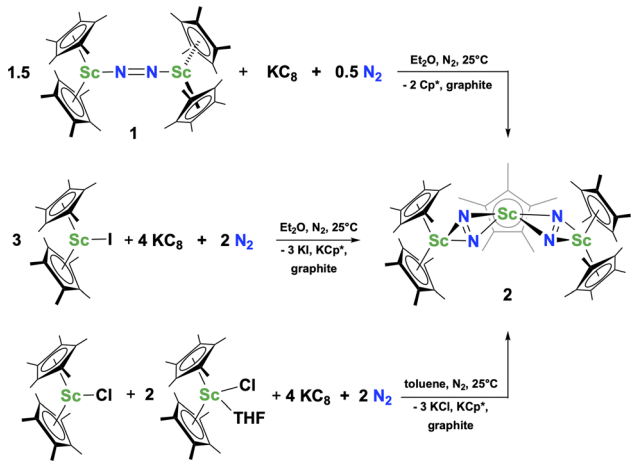

Scheme 1 Synthetic routes to Cp*Sc[(μ-η²:η²-N_2)ScCp*$_2$]$_2$, **2**.

reaction between $ScCl_3$ and 2 equiv. of KCp* in THF yielded crystals of both the solvated and unsolvated complexes, Cp*$_2$ScCl(THF) and Cp*$_2$ScCl, which were characterized by X-ray diffraction (see ESI†) and by comparison of their ^{1}H NMR spectra with literature values.[41,42] Complex **2** was not obtained by reacting either of these two compounds separately with KC_8 in toluene, but only reduction of the mixture of Cp*$_2$ScCl and Cp*$_2$ScCl(THF) in toluene provided complex **2** in good yield as shown in Scheme 1. Evidently, the presence of some THF facilitates the reduction of the Sc(III) complexes without causing decomposition of intermediates such as **1**.

In the X-ray crystal structure of **2**, the two Cp*$_2$Sc moieties are not related by symmetry and the two Sc_2N_2 cores do not have the rigorously planar side-on bridging structure that is usually seen in rare-earth element dinitrogen compounds.[9,26] Rather the Sc_2N_2 cores have a small distortion toward a butterfly structure which has been seen in some Zr and Hf side-on bridging (N=N)$^{2-}$ compounds.[9,43] The Sc_2N_2 fold angles in **2** are 7.47° for the N1–N2 moiety and 15.13° for the N3–N4 moiety.

The structural details of **2** are summarized in Table 2. The Sc–N distances are all in the narrow range of 2.140(2)–2.189(2) Å. Interestingly, within this range each nitrogen has either two shorter distances (for N2 and N3) or two longer distances (for N1 and N4), *i.e.* there is no short/long combination for each nitrogen donor atom as is sometimes seen in bridging ligands. The 2.18–2.20 Å Sc–Cent distances for the outer two scandium atoms, Sc1 and Sc3, are similar to the 2.17 Å value for the central Sc2, although the coordination numbers of the two types of scandium atoms are different. The 140.1° and 141.5° Cent–Sc–Cent angles of Sc1 and Sc3 are similar and smaller than the 146.7° angle in end-on **1**, but larger than the 131.0° angle in side-on [(C$_5$Me$_4$H)$_2$Sc]$_2$(μ-η²:η²-N_2).[12]

The ^{1}H NMR spectrum of **2** shows two singlets corresponding to the Cp* methyl groups in a 1 : 4 ratio, indicating that the two Cp*$_2$Sc groups are equivalent in solution. The ^{15}N NMR spectrum of the isotopically labeled compound Cp*Sc[(μ-η²:η²-$^{15}N_2$)ScCp*$_2$]$_2$, $^{15}N_2$, shows one signal at 771 ppm. This shift is further downfield than the 385 ppm shift of [(C$_5$Me$_4$H)$_2$Sc]$_2$(μ-η²:η²-N_2)[12] and the 495–569 range for [A$_2$(THF)Ln]$_2$(μ-η²:η²-N_2) (A = Cp*, C$_5$Me$_4$H, N(SiMe$_3$)$_2$; Ln = Y, La, Lu),[23] but these shifts obviously have a wide range.[10] The Raman spectrum of **2** shows a single N–N stretch at 1460 cm^{-1} which is shifted to 1415 cm^{-1} in the $^{15}N_2$ analogue. This stretching frequency is close in energy to those of other rare-earth metallocene side-on (N=N)$^{2-}$ compounds which have N–N stretches in the *ca.* 1400–1470 cm^{-1} range.[37]

Isolation of Cp*$_2$Sc(μ-η²:η²-N_2)ScI(THF)Cp*, 3

In previous attempts to isolate Cp* ligated Sc(II) species, Cp*$_2$ScI was treated with a combination of KC_8 and 18-crown-6 under an argon atmosphere and a crystal of the ligand redistribution

Table 2 Metrical parameters for $Cp^*Sc[(\mu\text{-}\eta^2\text{:}\eta^2\text{-}N_2)ScCp^*_2]_2$, **2**, and the side-on isomer of $Cp^*Sc(\mu\text{-}\eta^2\text{:}\eta^2\text{-}N_2)ScI(THF)Cp^*$, **3**

$Cp^*Sc[(\mu\text{-}\eta^2\text{:}\eta^2\text{-}N_2)ScCp^*_2]_2$, **2**				$Cp^*_2Sc(\mu\text{-}\eta^2\text{:}\eta^2\text{-}N_2)ScI(THF)Cp^*$, **3**	
Sc1–N1	2.178(2)	N1–N2	1.230(2)	N1–N2	1.246(5)
Sc1–N2	2.160(2)	N3–N4	1.233(2)	Sc1–N1	2.125(3)
Sc2–N1	2.189(2)	Sc1–Cent	2.20, 2.19	Sc1–N2	2.168(4)
Sc2–N2	2.177(2)	Sc2–Cent	2.17	Sc2–N1	2.184(3)
Sc2–N3	2.158(2)	Sc3–Cent	2.19, 2.18	Sc2–N2	2.185(4)
Sc2–N4	2.178(2)	Cent–Sc1–Cent	140.1	Sc1–I1	2.881(1)
Sc3–N3	2.140(2)	Cent–Sc3–Cent	141.5	Sc1–O1	2.231(3)
Sc3–N4	2.176(2)	(Sc1N1N2)–(N1N2Sc2)	7.47(5)°	Sc1–Cent	2.21
		(Sc2N3N4)–(N3N4Sc3)	15.13(6)°	Sc2–Cent	2.20, 2.20

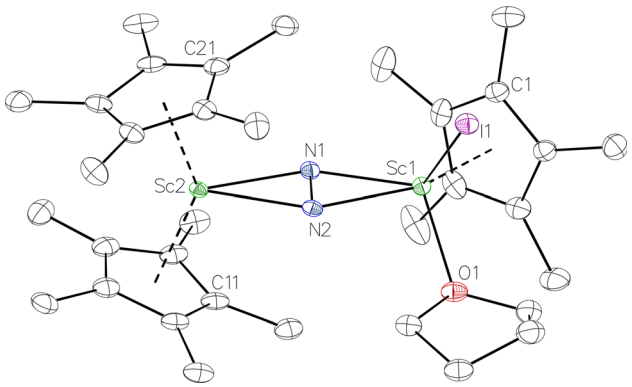

Fig. 4 Molecular structure of the major $Cp^*_2Sc(\mu\text{-}\eta^2\text{:}\eta^2\text{-}N_2)ScI(THF)Cp^*$ component of **3** with thermal ellipsoids shown at 30% and the $Sc(\mu\text{-}\eta^1\text{:}\eta^1\text{-}N_2)Sc$ disordered core and hydrogen atoms omitted for clarity.

product $[Cp^*_2Sc(crown)][Cp^*_2ScI_2]$ was isolated.[31] The analogous reaction investigated under N_2 atmosphere resulted again in the formation of **2**. However, the black precipitates from this reaction, presumably graphite and KCp*, had a green hue and were extracted with THF to afford a green solution. Removal of the solvent and recrystallization of the residue from *n*-hexane at −35 °C gave green crystals, which turned purple under the cold stream of the X-ray diffractometer, and were identified to be $Cp^*_2Sc(\mu\text{-}\eta^x\text{:}\eta^x\text{-}N_2)ScI(THF)Cp^*$ ($x = 1$, 2), **3**, Fig. 4.

The structure of **3** shows a disordered Sc–N_2–Sc core with 82% of the structure binding N_2 in a side-on fashion and the remainder binding end-on. For the major side-on component of the structure of **3**, $Cp^*_2Sc(\mu\text{-}\eta^2\text{:}\eta^2\text{-}N_2)ScI(THF)Cp^*$, the $(Cp^*_2Sc)^{1+}$ moiety involving Sc2 has metrical parameters that are very similar to those in complex **2**, Table 2. The 1.246(5) Å N–N distance is also similar. The $[Cp^*ScI(THF)]^{1+}$ moiety has a similar Sc1–Cent distance and one similar Sc–N distance, but the 2.125(3) Å Sc1–N1 distance is shorter than the other Sc–N distances in **2** and **3**. The N–N stretch of **3** appears at 1700 cm^{-1} in the Raman spectrum which is on the high end of the known rare-earth element $(N{=}N)^{2-}$ compounds.[37]

Small amounts of **3** could be reproducibly made by treating Cp^*_2ScI with KC_8 and 18-crown-6 in Et_2O according to eqn (2) and it was also obtained when 2.2.2-cryptand was used instead. The ^1H NMR spectrum of the material shows that **3** is isolated alongside varying amounts of an unidentified byproduct that appears at 1.93 ppm in C_6D_6. The use of a chelating agent appears necessary to generate **3**, as only **2** was isolated from the reduction of Cp^*_2ScI using 2 equiv. of KC_8 without 2.2.2-cryptand or 18-crown-6.

A green solution of **3** in toluene slowly changes color to red-purple when immersed in liquid nitrogen and reverts to green within several seconds of being removed from the liquid nitrogen. A movie of this transformation is in the ESI.† This temperature dependent change of color is reminiscent of the solid-state end-on to side-on yellow to green transformation observed for $[(R_2N)_3Nd(\mu\text{-}\eta^x\text{:}\eta^x\text{-}N_2)]^{2-}$ ($x = 1$,2).[27] Although a high yield synthesis of this compound has not been pursued, it is described here to show the existence of such hetero-ligated reduced dinitrogen complexes and as another example of solid state isomerization system.

Cp*Sc oxides

The scandium atoms in the crystal structure of **1** are disordered with 5% lying closer to the center of the Sc_2N_2 core. This could be indicative of a small portion of side-on bridging N_2 isomer in the crystal structure or a co-crystallized oxide product, $(Cp^*_2Sc)_2(\mu\text{-}O)$. Such $(Cp^*_2Ln)_2(\mu\text{-}O)$ complexes are common side products in Cp* rare-earth metal chemistry[23,44,45] and $[(R_2N)_3Ln(\mu\text{-}O)]^{2-}$ species were previously found in crystal structures of $[(R_2N)_3Ln(\mu\text{-}\eta^x\text{:}\eta^x\text{-}N_2)]^{2-}$ complexes.[27,28]

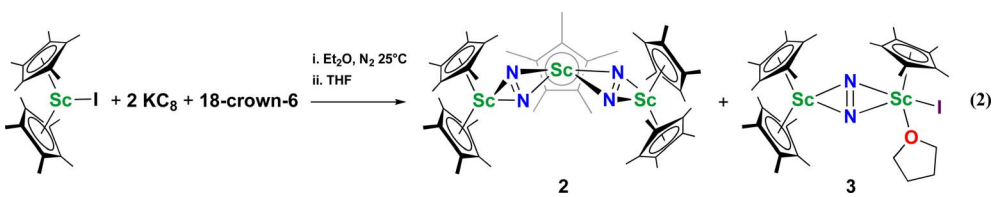

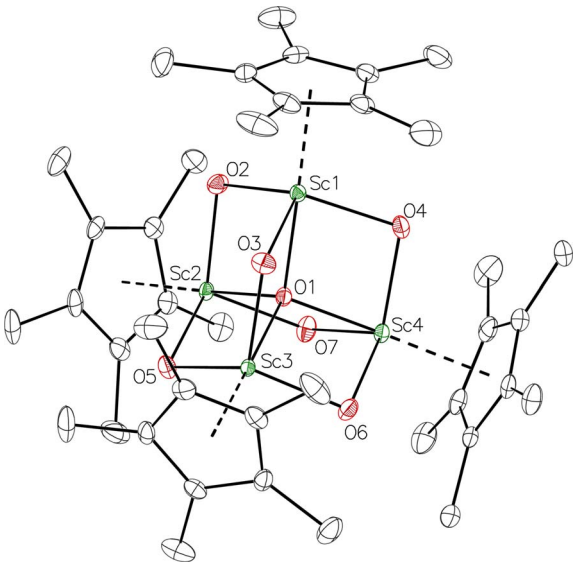

Fig. 5 Molecular structure of $(Cp^*Sc)_4(\mu_4\text{-}O)(\mu\text{-}OH)_6$, **4**, with ellipsoids drawn at 30% probability and hydrogen atoms omitted for clarity.

The 3.74(2) Å Sc···Sc distance in this minor component in the structure of **1** is much closer to the 3.80 Å Sc···Sc separation in the known oxide $[(C_5Me_4H)_2Sc]_2(\mu\text{-}O)$ than the 4.18 Å distance in the side-on $(N_2)^{2-}$ complex $[(C_5Me_4H)_2Sc]_2(\mu\text{-}\eta^2\text{:}\eta^2\text{-}N_2)$.[12] Notably, the titanium oxide $(Cp^*_2Ti)_2(\mu\text{-}O)$ has a similar Ti···Ti separation (3.816 Å) and crystallizes in the same space group (*I*222) as **1** with similar unit cell parameters.[46] A signal at 2.01 ppm is consistently present in the ^{1}H NMR spectra of purified samples of **1** in C_6D_6 and is possibly due to this oxide, $(Cp^*_2Sc)_2(\mu\text{-}O)$.

Since the reaction between Cp^*_2Sm and N_2O gave the bridging oxide product $(Cp^*_2Sm)_2(\mu\text{-}O)$,[44] we attempted to generate the scandium oxide this way starting from **1**. Treating a C_6D_6 solution of **1** with N_2O led to a rapid color change from dark blue to pale yellow and formation of a single product with a ^{1}H resonance at 2.01 ppm, lending further evidence that the oxide product is responsible for this signal. Similarly, the reaction of **2** with N_2O in C_6D_6 resulted in two new ^{1}H signals at 2.26 and 2.03 ppm in a 1 : 4 ratio indicating a different product is formed starting from **2**.

We have not yet been successful in isolating single crystals of the complex $(Cp^*_2Sc)_2(\mu\text{-}O)$ or of the side-on bridging N_2 isomer of **1** for comparison with the crystal structure of **1** reported above. In one attempt to grow crystals by slow evaporation of a C_6D_6 solution containing presumably the oxide $(Cp^*_2Sc)_2(\mu\text{-}O)$, several colorless crystals were obtained and identified by X-ray crystallography to be $(Cp^*Sc)_4(\mu_4\text{-}O)(\mu\text{-}OH)_6$, **4**, Fig. 5. This polyhydroxy species has a diamondoid core with a central μ_4-oxide and is further described in the ESI.† The formation of such polymetallic clusters containing $[Cp^*Ln]^{2+}$ vertices is common in rare-earth metal chemistry.[47,48]

Computational studies

Electronic structure calculations were performed on $Cp^*_2Sc[(\mu\text{-}\eta^1\text{:}\eta^1\text{-}N_2)ScCp^*_2]_2$, **1**, $Cp^*Sc[(\mu\text{-}\eta^2\text{:}\eta^2\text{-}N_2)ScCp^*_2]_2$, **2**, and $Cp^*_2Sc(\mu\text{-}\eta^2\text{:}\eta^2\text{-}N_2)ScI(THF)Cp^*$, **3** using density functional theory (DFT) with the TPSSh density functional[49,50] with Grimme's D3 dispersion correction,[51] including a Becke–Johnson damping function,[52] in the gas phase. Additionally, the resolution of the identity (RI-J) approximation was utilized.[53] Nonmetallic atoms were treated with def2-SV(P)[54] basis sets, while Sc was treated with triple-zeta quality basis sets def2-TZVP.[55,56] Additionally, each compound was optimized in the liquid phase using the TPSSh functional and the same basis sets as in the gas phase. The solvation effects of hexane were taken into account by applying the COSMO model[57] with a dielectric constant of 1.887 and an index of refraction of 1.3727. The optimized structures with the COSMO model were verified as local minima through vibrational analysis. The electronic spectra of each optimized compound were simulated using time-dependent density functional theory (TDDFT) calculations employing the non-orthonormal Krylov subspace method.[58] The validity of the computational protocol has been thoroughly tested and compared with X-ray structures and UV-visible spectra of rare-earth molecular complexes, as demonstrated in previous studies.[59] All calculations in this work were performed using the TURBOMOLE quantum chemistry package (version 7.8).[60] Complete details can be found in the ESI.†

The initial structures of **1–3** for DFT calculations were obtained from single crystal X-ray diffraction. In each case, the structural parameters calculated for the ground state structures were within a few degrees for angles and within 0.02–0.03 Å in distances as is typical for this level of computation.[59] The ground state assignment for each complex as described below is based on the relative energies of the different spin states, the agreement between calculated structural parameters and X-ray

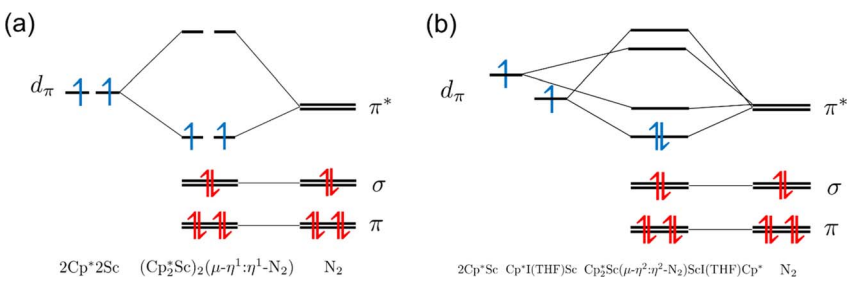

Fig. 6 Qualitative MO diagram for (a) $Cp^*_2Sc[(\mu\text{-}\eta^1\text{:}\eta^1\text{-}N_2)ScCp^*_2]_2$, **1**, and (b) the side-on component of **3**, $Cp^*_2Sc(\mu\text{-}\eta^2\text{:}\eta^2\text{-}N_2)ScI(THF)Cp^*$.

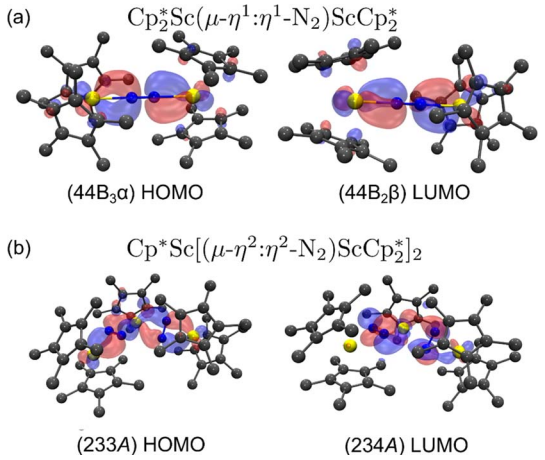

Fig. 7 (a) HOMO and LUMO of $Cp^*_2Sc[(\mu\text{-}\eta^1\text{:}\eta^1\text{-}N_2)ScCp^*_2]_2$, **1**; (b) HOMO and LUMO of $Cp^*Sc[(\mu\text{-}\eta^2\text{:}\eta^2\text{-}N_2)ScCp^*_2]_2$, **2**, using a contour value of 0.04. Hydrogen atoms are omitted for clarity.

data, and a comparison between the simulated and experimental electronic spectra. Detailed information on the possible spin states for these complexes are given in the ESI.†

For the end-on complex, **1**, DFT revealed that the triplet state is the ground state, while the singlet state is 0.26 eV (6.00 kcal mol^{-1}) higher in energy (see Table S10†). The qualitative MO diagram in Fig. 6 shows two unpaired electrons in the highest occupied molecular orbitals that are two degenerate orbitals that are mainly N_2 π* in character, but have Sc–N_2–Sc π bonding components, Fig. 7a. This bonding picture matches that of the end-on complex $[K(crypt)]_2\{[(R_2N)_3Sc]_2(\mu\text{-}\eta^1\text{:}\eta^1\text{-}N_2)\}$.[13] Analysis of the Kohn–Sham molecular orbitals suggests a strong interaction between the scandium 3d orbitals and the antibonding π* orbital of N_2 in the ScN_2Sc plane, leading to calculated and observed N–N and Sc–N bond lengths that are relatively shorter compared to other rare-earth dinitrogen complexes, Table 1. The analysis of spin density from the natural population indicates that the unpaired electrons are assigned to N p-orbitals and Sc d-orbitals with a value of 0.45 assigned to each orbital. This results in a triplet state and two-electron four-center $Sc(d_\pi)$–$N_2(\pi^*)$ bonding interactions between two Cp^*_2Sc fragments and N_2.

A calculation on the side-on variant of **1**, *i.e.* $(Cp^*_2Sc)_2(\mu\text{-}\eta^2\text{:}\eta^2\text{-}N_2)$, indicated that it is 0.415 eV (9.57 kcal mol^{-1}) higher in energy. In comparison, the side-on $\{[(R_2N)_3Sc]_2(\mu\text{-}\eta^2\text{:}\eta^2\text{-}N_2)\}^{2-}$ was previously calculated to be 12 kcal mol^{-1} less stable than the observed end-on $\{[(R_2N)_3Sc]_2(\mu\text{-}\eta^1\text{:}\eta^1\text{-}N_2)\}^{2-}$.[4]

For the side-on component of $Cp^*_2Sc(\mu\text{-}\eta^2\text{:}\eta^2\text{-}N_2)ScI(THF)Cp^*$, **3**, DFT calculations indicated that the singlet state is the ground state, while the triplet state is 1.16 eV (26.75 kcal mol^{-1}) higher in energy (see Table S15†). The qualitative MO diagram in Fig. 6b is similar to that of $[(C_5Me_4H)_2Sc]_2(\mu\text{-}\eta^2\text{:}\eta^2\text{-}N_2)$[12] and contains an electron pair in the HOMO formed from interaction of Sc 3d orbitals and an antibonding π* orbital of N_2. However, the LUMO of side-on **3** exhibits mixing between a Sc d orbital and a π* orbital of N_2 (see Fig. S17 and Table S9†), in contrast to the LUMO of $[(C_5Me_4H)_2Sc]_2(\mu\text{-}\eta^2\text{:}\eta^2\text{-}N_2)$.[12] Additionally, the end-on component of **3** was also evaluated by DFT calculations and is found to be 0.54 eV (12.45 kcal mol^{-1}) higher in energy. In the case of the $[(R_2N)_3Nd(\mu\text{-}\eta^x\text{:}\eta^x\text{-}N_2)]^{2-}$ dianion ($x = 1, 2$), the end-on isomer is favored at low temperature and converts to the side-on at around −100 °C in the solid state.[27]

DFT calculations on the trimetallic complex, **2**, indicated that the ground state is consistent with a singlet. Calculated structures with alternative triplet and quintet spin states are 0.97 (22.37 kcal mol^{-1}) and 2.22 eV (51.19 kcal mol^{-1}) higher in energy, respectively (see Table S13†). The HOMO of **2** displays characteristics consistent with two reduced N_2 ligands (see Fig. 7b and Table S19†), which is consistent with the Sc–N bond distances (Tables 2 and S13†). Hence, this complex has an electron pair in each of the two reduced dinitrogen ligands. Since rare-earth metal complexes of $(\mu\text{-}\eta^2\text{:}\eta^2\text{-}N_2)^{2-}$ ligands have an extensive two-electron reduction chemistry,[61–63] complex **2** could conceivably be a four-electron reductant.

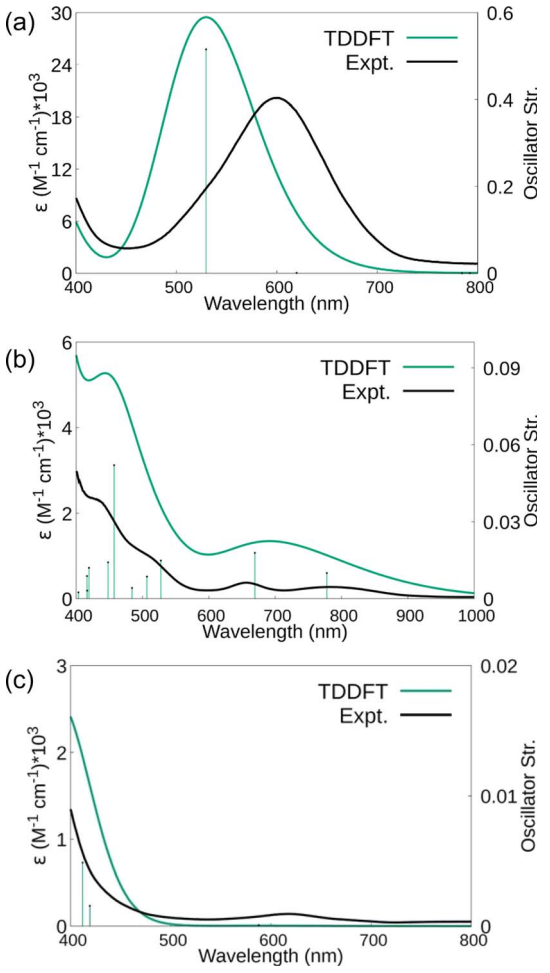

Fig. 8 Simulated and experimental (Et_2O) UV-visible absorbance spectra of (a) $(Cp^*_2Sc)_2(\mu\text{-}\eta^1\text{:}\eta^1\text{-}N_2)$, **1**, (b) $Cp^*Sc[(\mu\text{-}\eta^2\text{:}\eta^2\text{-}N_2)ScCp^*_2]_2$, **2**, and (c) the side-on isomer of **3**, $Cp^*_2Sc(\mu\text{-}\eta^2\text{:}\eta^2\text{-}N_2)ScCp^*I(THF)$. A Gaussian spectral line shape with a width of 0.2 eV was employed in each case.

The electronic spectra were simulated using TDDFT calculations and are compared with the experimental spectra in Fig. 8. Comparisons of the calculated spectra for different spin states are given in the ESI.† As shown in Fig. 8, the calculated spectra match the observed data well. For **1**, the main absorption band is due to electronic transitions corresponding to degenerate ($44B_2$ alpha) HOMO and ($44B_3$ alpha) HOMO-1 with Sc(d_π)-N_2(π^*) character to ($45B_3$ alpha) LUMO+6 and ($45B_2$ alpha) LUMO+7 with predominantly d character, respectively. Similarly, for **2** and **3**, the significant transitions are due to transitions with similar characters (see Tables S19–S22†).

Raman shifts were also calculated for **1–3** and scaled by a factor of 0.95 to account for anharmonicities and basis set incompleteness.[64] For end-on **1**, the calculated value was 1661 cm^{-1} compared to the 1595 cm^{-1} experimental value. For side-on **2**, the calculations indicated two stretching vibrations at lower energies, 1484 and 1544 cm^{-1}. A lower energy absorbance is observed at 1460 cm^{-1}, but only one band is observed under the experimental conditions. For **3**, the 1700 cm^{-1} experimentally observed stretch is in between the 1515 cm^{-1} calculated estimate for the side-on isomer and the 1737 cm^{-1} calculated stretch for the end-on isomer. The observed band is closer to the end-on calculation and higher than that expected for the solid-state structure that was predominantly side-on. However, it is possible that laser heating of the sample under the Raman experimental conditions generates more end-on isomer *in situ*.

Discussion

The preliminary reactivity previously observed in reductions of Cp^*_2ScI with KC_8 under argon[31] is further supported by the reactivity observed under dinitrogen reported here. Under argon, EPR and C–H bond reactivity data indicated the formation of a highly reactive red Sc(II) complex, possibly Cp^*_2Sc, but this species has not yet been isolated or crystallographically characterized.[31] It would be expected that a species like Cp^*_2Sc could reduce N_2 and indeed the Cp^*_2ScI/KC_8 system forms the bimetallic $(N{=}N)^{2-}$ complexes $(Cp^*_2Sc)_2(\mu\text{-}\eta^1{:}\eta^1\text{-}N_2)$, **1**, and $Cp^*_2Sc(\mu\text{-}\eta^2{:}\eta^2\text{-}N_2)ScCp^*I(THF)$, **3**, as well as the trimetallic species $Cp^*Sc[(\mu\text{-}\eta^2{:}\eta^2\text{-}N_2)ScCp^*_2]_2$, **2**. This doubles the number of previously characterized reduced dinitrogen complexes of scandium. In addition, to our knowledge complex **2** is the first dinitrogen complex of any metal in the periodic table that contains two side-on $(N{=}N)^{2-}$ ligands bound to the same metal.[32,33]

The end-on coordination mode found in $(Cp^*_2Sc)_2(\mu\text{-}\eta^1{:}\eta^1\text{-}N_2)$ contrasts with the side-on binding found with the tetramethylcyclopentadienyl scandium analog, $[(C_5Me_4H)_2Sc]_2(\mu\text{-}\eta^2{:}\eta^2\text{-}N_2)$, as well as the Cp* samarium analog, $(Cp^*_2Sm)_2(\mu\text{-}\eta^2{:}\eta^2\text{-}N_2)$.[15] Compared to either of these, there is more steric crowding in $(Cp^*_2Sc)_2(\mu\text{-}\eta^1{:}\eta^1\text{-}N_2)$ due to the larger ligand *versus* C_5Me_4H and the smaller metal *versus* Sm, which evidently leads to the end-on binding. The preference for side-on coordination in $Cp^*Sc[(\mu\text{-}\eta^2{:}\eta^2\text{-}N_2)ScCp^*_2]_2$, **2**, and $Cp^*_2Sc(\mu\text{-}\eta^2{:}\eta^2\text{-}N_2)ScCp^*I(THF)$, **3**, as well as in $\{[^n BuC(N^iPr)_2](Cp^*)Sc\}_2(\mu\text{-}\eta^2{:}\eta^2\text{-}N_2)$ is consistent with this steric rationale since all of these complexes have less bulky ligand sets. The end-on structure of $[K(crypt)]_2\{[(R_2N)_3Sc]_2(\mu\text{-}\eta^1{:}\eta^1\text{-}N_2)\}$, which has three bulky amide groups per scandium, also fits this picture.

The Raman shift of the N–N stretch in **1** is on the low end of values observed for end-on rare-earth metal $(N{=}N)^{2-}$ complexes, Table 1, but it is consistent with an N=N double bond. All of these shifts for end-on coordination are higher in energy than shifts observed for side-on rare-earth metal species which are in the range of 1413–1473 cm^{-1},[37] along with that of **2** (1460 cm^{-1}).

The formation of the first example of a bis(side-on) $(N{=}N)^{2-}$ trimetallic complex, **2**, was unexpected. The fact that this can be made both sequentially from **1** and directly from Cp^*_2ScI and $Cp^*_2ScCl/Cp^*_2ScCl(THF)$ suggests it is a rather favorable reaction product in this system. The reaction of **1** to form **2** in Scheme 1 requires the loss of a Cp* ligand during the KC_8 reduction. This may prove to be a general reaction of KC_8 with rare-earth metal Cp* complexes, since several examples of mono-Cp* ligated complexes were recently reported from KC_8 reductions of Cp^*_2Ln bipyridyl complexes.[65] The mechanism for the conversion of **1** to **2** is not obvious since the net stoichiometry in Scheme 1 is complicated and end-on to side-on isomerization is involved. The DFT calculations show that although the LUMO of **1** is consistent with the targeted $(N_2)^{3-}$ ligand, it is quite high in energy at 1.49 eV (34.36 kcal mol^{-1}) above the HOMO. Hence, this species may be unstable with respect to further reactions to form **2**. The LUMO of **1** also has a significant contribution from the scandium d-orbitals, while in compounds which have been successfully reduced, *e.g.* $\{[(Me_3Si)_2N]_2(THF)Y\}_2(\mu\text{-}\eta^2{:}\eta^2\text{-}N_2)$[29] and $\{[^n BuC(N^iPr)_2]Cp^*Sc\}_2(\mu\text{-}\eta^2{:}\eta^2\text{-}N_2)$,[14] the LUMOs are localized on the $(N{=}N)^{2-}$ moiety.

Conclusion

Although dinitrogen reduction chemistry with the first metal in the transition series, scandium, has not been extensively studied, this metal has generated unexpected results in this area. Reduction of Cp^*_2ScI and Cp^*_2ScCl under dinitrogen leads not only to the bimetallic scandium $(N{=}N)^{2-}$ complexes, $(Cp^*_2Sc)_2(\mu\text{-}\eta^1{:}\eta^1\text{-}N_2)$, **1**, and $Cp^*_2Sc(\mu\text{-}\eta^2{:}\eta^2\text{-}N_2)ScCp^*I(THF)$, **3**, but also to the unprecedented trimetallic species $Cp^*Sc[(\mu\text{-}\eta^2{:}\eta^2\text{-}N_2)ScCp^*_2]_2$, **2**. Clearly, scandium has a more extensive chemistry with dinitrogen than the three examples previously in the literature.[12–14] Isolation of a Sc(II) precursor such as Cp^*_2Sc is not necessary to access the scandium dinitrogen complexes and it is anticipated that other Cp*-ligated scandium reduced dinitrogen complexes should be synthetically accessible. Complexes **1–3** are expected to have a rich reaction chemistry based on previous studies of $(N{=}N)^{2-}$ reactivity.[61–63]

Data availability

Experimental procedures, X-ray crystallographic details, NMR and infrared spectroscopy data, and computational details are available in the ESI.† CCDC 2324189, 2344840, 2344841, and

2348488–2348490 contain the supplementary crystallographic data for this paper.

Author contributions

JDQ, ZX, and WJE provided the original concept. JDQ and QEG synthesized and characterized the compounds at UCI under the supervision of WJE and collected X-ray data under the supervision of JWZ. QY synthesized and characterized compounds at PKU under the supervision of ZX. Computations were done by AR and DKN under the supervision of FF. JDQ, AR, QY, ZX, and WJE wrote the manuscript with contributions from all authors. Funding was obtained by ZX, FF, and WJE.

Conflicts of interest

The authors declare no competing financial interest. Principal Investigator Filipp Furche has an equity interest in TURBOMOLE GmbH. The terms of this arrangement have been reviewed and approved by the University of California, Irvine, in accordance with its conflict of interest policies.

Acknowledgements

We thank the U. S. National Science Foundation for support of this research under CHE-2154255 (to W. J. E for the experimental research) and CHE-2102568 (to F. F. for the theoretical studies) and National Natural Science Foundation of China (No. 21988101, to Z. X.). A. R. acknowledges support from an Eddleman Quantum Institute Fellowship. We also thank Dr D. Fishman and Marcus Marracci for collection of the Raman spectra.

References

1 J. Chatt, J. R. Dilworth and R. L. Richards, *Chem. Rev.*, 1978, **78**, 589–625.
2 Y. Nishibayashi, *Inorg. Chem.*, 2015, **54**, 9234–9247.
3 J. G. Chen, R. M. Crooks, L. C. Seefeldt, K. L. Bren, R. M. Bullock, M. Y. Darensbourg, P. L. Holland, B. Hoffman, M. J. Janik, A. K. Jones, M. G. Kanatzidis, P. King, K. M. Lancaster, S. V. Lymar, P. Pfromm, W. F. Schneikder and R. R. Schrock, *Science*, 2018, **360**, eaar6611.
4 S. Kim, F. Loose and P. J. Chirik, *Chem. Rev.*, 2020, **120**, 5637–5681.
5 M. J. Chalkley, M. W. Drover and J. C. Peters, *Chem. Rev.*, 2020, **120**, 5582–5636.
6 A. D. Allen and C. V. Senoff, *Chem. Commun.*, 1965, 621–622.
7 D. F. Harrison, E. Weissberger and H. Taube, *Science*, 1968, **159**, 320–322.
8 K. Jonas, *Angew. Chem., Int. Ed.*, 1973, **12**, 997–998.
9 D. Singh, W. R. Buratto, J. F. Torres and L. J. Murray, *Chem. Rev.*, 2020, **120**, 5517–5581.
10 E. A. MacLachlan and M. D. Fryzuk, *Organometallics*, 2006, **25**, 1530–1543.
11 C. R. Groom, I. J. Bruno, M. P. Lightfoot and S. C. Ward, *Acta Crystallogr., Sect. B: Struct. Sci., Cryst. Eng. Mater.*, 2016, **72**, 171–179.
12 S. Demir, S. E. Lorenz, M. Fang, F. Furche, G. Meyer, J. W. Ziller and W. J. Evans, *J. Am. Chem. Soc.*, 2010, **132**, 11151–11158.
13 D. H. Woen, G. P. Chen, J. W. Ziller, T. J. Boyle, F. Furche and W. J. Evans, *J. Am. Chem. Soc.*, 2017, **139**, 14861–14864.
14 Z.-J. Lv, Z. Huang, W.-X. Zhang and Z. Xi, *J. Am. Chem. Soc.*, 2019, **141**, 8773–8777.
15 W. J. Evans, T. A. Ulibarri and J. W. Ziller, *J. Am. Chem. Soc.*, 1988, **110**, 6877–6879.
16 W. J. Evans, N. T. Allen and J. W. Ziller, *J. Am. Chem. Soc.*, 2001, **123**, 7927–7928.
17 W. J. Evans, N. T. Allen and J. W. Ziller, *Angew. Chem., Int. Ed.*, 2002, **41**, 359–361.
18 W. J. Evans, G. Zucchi and J. W. Ziller, *J. Am. Chem. Soc.*, 2003, **125**, 10–11.
19 W. J. Evans, D. S. Lee and J. W. Ziller, *J. Am. Chem. Soc.*, 2004, **126**, 454–455.
20 W. J. Evans, D. S. Lee, D. B. Rego, J. M. Perotti, S. A. Kozimor, E. K. Moore and J. W. Ziller, *J. Am. Chem. Soc.*, 2004, **126**, 14574–14582.
21 W. J. Evans, D. S. Lee, C. Lie and J. W. Ziller, *Angew. Chem., Int. Ed.*, 2004, **43**, 5517–5519.
22 W. J. Evans, D. S. Lee, M. A. Johnston and J. W. Ziller, *Organometallics*, 2005, **24**, 6393–6397.
23 W. J. Evans, D. B. Rego and J. W. Ziller, *Inorg. Chem.*, 2006, **45**, 10790–10798.
24 F. Jaroschik, A. Momin, F. Nief, X.-F. Le Goff, G. B. Deacon and P. C. Junk, *Angew. Chem., Int. Ed.*, 2009, **48**, 1117–1121.
25 B. M. Schmiege, J. W. Ziller and W. J. Evans, *Inorg. Chem.*, 2010, **49**, 10506–10511.
26 W. J. Evans and D. S. Lee, *Can. J. Chem.*, 2005, **83**, 375–384.
27 A. B. Chung, D. Rappoport, J. W. Ziller, R. E. Cramer, F. Furche and W. J. Evans, *J. Am. Chem. Soc.*, 2022, **144**, 17064–17074.
28 A. J. Ryan, S. G. Balasubramani, J. W. Ziller, F. Furche and W. J. Evans, *J. Am. Chem. Soc.*, 2020, **142**, 9302–9313.
29 W. J. Evans, M. Fang, G. Zucchi, F. Furche, J. W. Ziller, R. M. Hoekstra and J. I. Zink, *J. Am. Chem. Soc.*, 2009, **131**, 11195–11202.
30 M. Fang, J. E. Bates, S. E. Lorenz, D. S. Lee, D. B. Rego, J. W. Ziller, F. Furche and W. J. Evans, *Inorg. Chem.*, 2011, **50**, 1459–1469.
31 J. D. Queen, L. M. Anderson-Sanchez, C. R. Stennett, A. Rajabi, J. W. Ziller, F. Furche and W. J. Evans, *J. Am. Chem. Soc.*, 2024, **146**, 3279–3292.
32 R. Duchateau, S. Gambarotta, N. Beydoun and C. Bensimon, *J. Am. Chem. Soc.*, 1991, **113**, 8986–8988.
33 D. N. Huh, R. F. Koby, Z. E. Stuart, R. J. Dunscomb, N. D. Schley and I. A. Tonks, *Chem. Sci.*, 2022, **13**, 13330–13337.
34 R. D. Sanner, J. M. Manriquez, R. E. Marsh and J. E. Bercaw, *J. Am. Chem. Soc.*, 1976, **98**, 8351–8357.
35 Y.-T. Hung, G. P. A. Yap and K. H. Theopold, *Polyhedron*, 2019, **157**, 381–388.

36 A. Mondal, C. G. T. Price, J. Tang and R. A. Layfield, *J. Am. Chem. Soc.*, 2023, **145**, 20121–20131.
37 M. E. Fieser, D. H. Woen, J. F. Corbey, T. J. Mueller, J. W. Ziller and W. J. Evans, *Dalton Trans.*, 2016, **45**, 14634–14644.
38 D. F. Evans, *J. Chem. Soc.*, 1959, 2003–2005.
39 S. K. Sur, *J. Magn. Reson.*, 1989, **82**, 169–173.
40 G. A. Bain and J. F. Berry, *J. Chem. Educ.*, 2008, **85**, 532.
41 M. E. Thompson, S. M. Baxter, A. R. Bulls, B. J. Burger, M. C. Nolan, B. D. Santarsiero, W. P. Schaefer and J. E. Bercaw, *J. Am. Chem. Soc.*, 1987, **109**, 203–219.
42 W. Huynh, D. B. Culver, H. Tafazolian and M. P. Conley, *Dalton Trans.*, 2018, **47**, 13063–13071.
43 M. Hirotsu, P. P. Fontaine, P. Y. Zavalij and L. R. Sita, *J. Am. Chem. Soc.*, 2007, **129**, 12690–12692.
44 W. J. Evans, J. W. Grate, I. Bloom, W. E. Hunter and J. L. Atwood, *J. Am. Chem. Soc.*, 1985, **107**, 405–409.
45 W. J. Evans, B. L. Davis, G. W. Nyce, J. M. Perotti and J. W. Ziller, *J. Organomet. Chem.*, 2003, **677**, 89–95.
46 J. Pinkas, I. Císařová, R. Gyepes, J. Kubišta, M. Horáček and K. Mach, *Organometallics*, 2013, **32**, 6306–6314.
47 W. J. Evans, N. T. Allen, M. A. Greci and J. W. Ziller, *Organometallics*, 2001, **20**, 2936–2937.
48 T. Shima and Z. Hou, *J. Am. Chem. Soc.*, 2006, **128**, 8124–8125.
49 V. N. Staroverov, G. E. Scuseria, J. Tao and J. P. Perdew, *J. Chem. Phys.*, 2003, **119**, 12129–12137.
50 M. K. Armbruster, F. Weigend, C. van Wüllen and W. Klopper, *Phys. Chem. Chem. Phys.*, 2008, **10**, 1748–1756.
51 S. Grimme, J. Antony, S. Ehrlich and H. Krieg, *J. Chem. Phys.*, 2010, **132**, 154104.
52 S. Grimme, S. Ehrlich and L. Goerigk, *J. Comput. Chem.*, 2011, **32**, 1456–1465.
53 K. Eichkorn, O. Treutler, H. Öhm, M. Häser and R. Ahlrichs, *Chem. Phys. Lett.*, 1995, **240**, 283–290.
54 A. Schäfer, H. Horn and R. Ahlrichs, *J. Chem. Phys.*, 1992, **97**, 2571–2577.
55 F. Weigend and R. Ahlrichs, *Phys. Chem. Chem. Phys.*, 2005, **7**, 3297–3305.
56 R. Gulde, P. Pollak and F. Weigend, *J. Chem. Theory Comput.*, 2012, **8**, 4062–4068.
57 A. Klamt and G. Schüürmann, *J. Chem. Soc., Perkin Trans. 2*, 1993, 799–805.
58 F. Furche, B. T. Krull, B. D. Nguyen and J. Kwon, *J. Chem. Phys.*, 2016, **144**, 174105.
59 A. Rajabi, R. Grotjahn, D. Rappoport and F. Furche, *Dalton Trans.*, 2024, **53**, 410–417.
60 Y. J. Franzke, C. Holzer, J. H. Andersen, T. Begušić, F. Bruder, S. Coriani, F. Della Sala, E. Fabiano, D. A. Fedotov, S. Fürst, S. Gillhuber, R. Grotjahn, M. Kaupp, M. Kehry, M. Krstić, F. Mack, S. Majumdar, B. D. Nguyen, S. M. Parker, F. Pauly, A. Pausch, E. Perlt, G. S. Phun, A. Rajabi, D. Rappoport, B. Samal, T. Schrader, M. Sharma, E. Tapavicza, R. T. Treß, V. Voora, A. Wodyński, J. M. Yu, B. Zerulla, F. Furche, C. Hattig, M. Sierka, D. P. Tew and F. Weigend, *J. Chem. Theory Comput.*, 2023, **19**, 6859–6890.
61 W. J. Evans, D. S. Lee, J. W. Ziller and N. Kaltsoyannis, *N. J. Am. Chem. Soc.*, 2006, **128**, 14176–14184.
62 W. J. Evans, J. R. Walensky, T. M. Champagne, J. W. Ziller, J. W. A. G. DiPasquale and A. L. Rheingold, *J. Organomet. Chem.*, 2009, **694**, 1238–1243.
63 S. E. Lorenz, B. M. Schmiege, D. S. Lee, J. W. Ziller and W. J. Evans, *Inorg. Chem.*, 2010, **49**, 6655–6663.
64 K. P. Huber and G. Herzberg, Constants of Diatomic Molecules (data prepared by J. W. Gallagher, and R. D. Johnson III), in *NIST Chemistry WebBook, NIST Standard Reference Database No. 69*, ed. P. J. Linstrom and W. G. Mallard, National Institute of Standards and Technology, Gaithersburg MD, 2009, **https://webbook.nist.gov/**, (retrieved December 6, 2009).
65 C. R. Stennett, J. W. Ziller and W. J. Evans, *Eur. J. Inorg. Chem.*, 2024, e202300732.